Knockout of ccr2 alleviates photoreceptor cell death in a model of retinitis pigmentosa

Congrong Guo,[1,2] Atsushi Otani,[1] Akio Oishi,[1] Hiroshi Kojima,[1] Yukiko Makiyama,[1] Satoko Nakagawa[1] and Nagahisa Yoshimura[1]

[1] Department of Ophthalmology, Kyoto University Graduate School of Medicine, Kyoto 606-8507, JAPAN

[2] Department of Ophthalmology, Second Hospital of Hebei Medical University, Hebei, China

Address correspondence to:

Atsushi Otani, MD, PhD

Department of Ophthalmology, Kyoto University Graduate School of Medicine

54-Kawaharacho, Shogoin, Sakyo-ku, Kyoto 606-8507, JAPAN

E-mail: otan@kuhp.kyoto-u.ac.jp;

Fax: +81-75-752-0933;

Tel: +81-75-751-3248

Congrong Guo
guocongrong@msn.com
Akio Oishi
aquio@kuhp.kyoto-u.ac.jp
Hiroshi Kojima
hkojima@kuhp.kyoto-u.ac.jp
Yukiko Makiyama
yukimaki@kuhp.kyoto-u.ac.jp
Satoko Nakagawa
satomai@kuhp.kyoto-u.ac.jp
Nagahisa Yoshimura
nagaeye@kuhp.kyoto-u.ac.jp

Abstract

Neuroinflammation involving CC chemokines such as monocyte chemoattractant protein-1 (MCP-1) has been demonstrated in the pathological process of retinitis pigmentosa (RP), an inherited degenerative retinal disease. However, the mechanism of MCP-1 and its receptor CCR2 involvement in the disease remains unclear. To investigate the role of MCP1/CCR2 in RP pathogenesis, ccr2 mutant RP mice (ccr2−/− rd10) were created and analyzed. The expression of MCP-1, RANTES, stromal cell-derived factor (SDF-1), and tumor necrosis factor-α (TNF-α) in the retinas of wild-type, rd10, and ccr2−/− rd10 mice was analyzed using quantitative RT-PCR. Photoreceptor apoptosis (TUNEL staining) and the number of microglia (positive for the F4/80 antibody) in the retina were examined. Retinal function was assessed using electroretinograms, and the structure of the whole retina was analyzed from images obtained using optical coherence tomography (OCT) and by histological examination. The expression levels of MCP-1, RANTES, and SDF-1 increased with time in the rd10 mice but not in the wild-type mice. Rearing the mice in the dark prevented degeneration and resulted in thicker photoreceptor layers at each time point. In those mice, the peaks of chemokine expression shifted to a later time with degeneration, suggesting that the expression of these chemokines was induced during the progression of degeneration. Although the difference was not so obvious, the retina in the ccr2−/− rd10 mice was consistently and significantly thicker than that in the

rd10 (ccr2+/+ rd10) mice at all time points. Rhodopsin gene expression was also higher in the ccr2−/− rd10 mice than in rd10 (ccr2+/+ rd10) mice, suggesting photoreceptor survival in the former. Retinal function was also better preserved in the ccr2−/− rd10 mice than in the rd10 mice. The number of microglia in the retinas of the ccr2−/− rd10 mice was significantly lower than that in the retinas of the rd10 mice. Interestingly, the MCP-1 induction that was observed in the retinas of the rd10 mice was diminished in the retinas of the ccr2−/− rd10 mice. Our results suggest that the MCP-1/CCR2 system plays a role in retinal degeneration in rd mouse retinas. Retinal MCP-1 expression in the rd mouse retina may be partially controlled by ccr2-positive circulating cells.

Keywords: CCR2; MCP-1; Chemokines; Retinitis pigmentosa; Photoreceptor

1. Introduction

Retinitis pigmentosa (RP) is a family of inherited diseases characterised by night blindness and loss of peripheral vision followed by progressive loss of central vision.(Hartong et al., 2006) To date, 172 genes have been implicated in RP-related conditions, indicating the genetic diversity of this group of diseases (RetNet database: http://www.sph.uth.tmc.edu/retnet/). As for many other neurodegenerative diseases, no effective therapy for this inherited form of blindness is known.

The pathogenesis of neurodegenerative diseases in the central nervous system (CNS) has been suggested to be closely associated with chronic inflammatory processes (Sriram, 2011). Microglia, which originate from circulating bone marrow (BM)-derived monocytes, are key players in CNS inflammatory processes (Epstein, 1998; Matyszak, 1998; Raine, 1994; Saijo and Glass, 2011). Activated microglial cells, which express tumor necrosis factor-α (TNF-α), migrate into the retina during retinal degeneration, suggesting that these cells trigger photoreceptor cell death (Zeng et al., 2005). On the other hand, microglia have also been reported to secrete neurotrophic factors and promote photoreceptor survival in a light-induced retinal degeneration model (Harada et al., 2002). Thus, the role played by microglia in inflammatory processes related to retinal degeneration remains unclear.

Chemokines are immune signaling molecules that comprise a family of cytokines. They control inflammation by functioning as chemoattractants that

recruit inflammatory cells to the appropriate extravascular sites of inflammation (Bennett et al., 2011; Huang et al., 2000; Lawrence and Kim, 2000; Xia and Hyman, 1999). Structurally, chemokines can be divided into 4 subfamilies (CXC, CC, XC, and CX3C) depending on the number and spacing of amino acids (X) located between the first 2 conserved cysteine residues (Zola et al., 2003; Luster et al., 1998). Monocyte chemoattractant protein-1 (MCP-1 or CCL2), one of the most studied CC chemokines, is secreted primarily by monocytes, macrophages, neurons, astrocytes, and microglia (Coughlan et al., 2000; Glabinski et al., 1996; Gourmala et al., 1997; Gu et al., 1999; Simpson et al., 1998). The production of MCP-1 is also observed in the retinal cells including RPE, subretinal macrophages and muller cells (Chen et al., 2008; Ma et al., 2009; Nakazawa et al., 2007). MCP-1 induces circulating monocytes to migrate into the tissue to become tissue macrophages or microglia (Gu et al., 1999). Studies have also suggested that MCP-1 plays an important role in the neuroinflammatory processes of degenerative CNS diseases (Conductier et al., 2010; Gerard and Rollins, 2001) such as autoimmune encephalomyelitis (Fife et al., 2000; Huang et al., 2001; Izikson et al., 2000), Alzheimer disease (Hickman and El Khoury, 2010), ischemic neuropathy (Kim et al., 2005), and trauma (Semple et al., 2010). Increased expression of MCP-1 and another CC chemokine, namely, RANTES (Regulated upon Activation, Normal T-cell Expressed, and Secreted) has also been reported in retinal degeneration (Zeng et al., 2005).

Chemokines are remarkably diverse in their functions and production and have therefore also been grouped into functional subfamilies termed “inflammatory,” “homeostatic,” and “dual-function” chemokines (Moser et al., 2004). We previously reported a neuroprotective role for the homeostatic chemokine stromal cell-derived factor-1 (SDF-1) (Otani et al., 2004; Sasahara et al., 2008). Recently, Chen et al. (2012) reported that CCL2 or CCR2-deficient mice develop degenerative retinal changes with age. In another report, although accelerated accumulation of macrophages was observed, CCL2-deficient mice showed no particular retinal change with age (Luhmann et al., 2009). It is still controversial in the role of MCP-1/CCR2 system of retina and the differences in the results may be explained by the presence of additional factors including pathologic conditions, light exposure and other stressors. In the present study, we investigated the role of the inflammatory chemokine MCP-1 in the pathology of inherited retinal degeneration.

2. Materials and Methods

2.1 Animals

All animals were used and cared for in accordance with the Association for Research in Vision and Ophthalmology Statement for the Use of Animals in Ophthalmic and Vision Research and the Guidelines for Animal Experiments of Kyoto University. All experiments were conducted with the approval of the Animal Research Committee, Graduate School of Medicine, Kyoto University.

C57BL/6 (B6) (Japan SLC, Inc., Shizuoka, Japan), B6.CXB1-Pde6brd10/J

(rd10), and B6.129S4-Ccr2 (tm1 Ifc)/J (ccr2−/−) mice (The Jackson Laboratory, Bar Harbor, ME) were used. Further, ccr2−/− rd10 mice were generated by crossing ccr2−/− and rd10 mice. All mice were maintained under a 12-h light/dark cycle under the control of animal facility. The light was conventional fluorescent light and the intensity was around 150 lux in the cage. A subset of the rd10 mice was raised in 24-h total darkness.

2.2 Genotyping

Genotypes were determined by PCR analysis of tail samples. ccr2 (NM_009915.2) genotypes were determined by discriminatory PCR analysis. rd10 genotypes were determined using restriction fragment length polymorphism (RFLP) analysis related to the rd10 mutation: c560 C > T in the Pde6b gene (Chang et al., 2007) destroys the HhaI site. We used the following pairs of primers: wild-type ccr2 forward (5′-CCACAGAATCAAAGGAAATGG-3′) and reverse (5′-CCAATGTGATAGAGCCCTGTG-3′), mutant ccr2 forward (5′-CTTGGGTGGAGAGGCTATTC-3′) and reverse (5′-AGGTGAGATGACAGGAGATC-3′), and Pde6b forward (5′-CTTTCTATTCTCTGTCAGCAAAGC-3′) and reverse (5′-TTGCTAGGACTGGATACACAC-3′). The PCR cocktail (50 µl/sample) contained 10 µl Phusion HF Buffer (5×) (New England Biolabs, Ipswich, MA), 4 µl 2.5 mM dNTP mixture (TAKARA, Otsu, Japan), 0.25 µl of 100 µM forward and reverse primers each, 100 ng sample genomic DNA, 0.25 µl Phusion DNA

Polymerase (New England BioLabs), and dH2O to make up the volume to 50 µl. The PCR cycle was performed as follows: 98 °C for 30 s; 35 cycles of 98 °C for 5 s, 65 °C for 10 s, and 72 °C for 10 s; and a final extension step at 72 °C for 1 min. For amplification of Pde6b, the annealing temperature was set to 61 °C. HhaI digestion was carried out in a 30-µl reaction mixture comprising 26 µl of the PCR product (Pde6b), 3 µl of 10× NE Buffer, 0.3 µl 100× BSA, and 14 units of HhaI (New England BioLabs). The products were separated by electrophoresis in a 2% (ccr2) or 4% (Pde6b) agarose gel and stained with ethidium bromide for visualization.

2.3 Real-time RT-PCR assay

Total mRNA was prepared from whole mouse retinas by using an RNeasy kit (Qiagen, Tokyo, Japan), and they were transcribed using the First-Strand cDNA synthesis kit (GE Healthcare, Tokyo, Japan). Real-time PCR (40 cycles, ABI Prism 7000 sequence detection system, Applied Biosystems, Carlsbad, California) was performed using TaqMan PreAmp master mix, fluorogenic TaqMan MGB probes, and Assay-on-Demand™ Gene Expression primers for MCP-1 (Mm99999056_m1), RANTES (Mm01302428_m1), SDF-1 (Mm00457276_m1), TNF-α (Mm099999068_m1), and rhodopsin (Mm01184405_ m1) (Applied Biosystems, Tokyo, Japan). β-Actin was used as the internal control for each sample. The fold changes in the mRNA level were calculated using the comparative Ct method (Frossard et al., 2011).

2.4 Recording of electroretinograms (ERGs)

After overnight dark adaptation, mice were anesthetized by intraperitoneal injection of 50 μg/kg ketamine and 10 μg/kg xylazine. The pupils were fully dilated with eye drops containing 0.4% tropicamide and 0.5% phenylephrine hydrochloride. During electroretinogram (ERG) recording, the mice were kept on a heating pad in order to maintain their body temperature. The ERGs were recorded using PowerLab 2/25 (AD Instruments, Bella Vista, Australia) with gold wire loops placed on the right cornea. Reference electrodes were placed in the cheek and ground leads were placed in the hip.

Full-field scotopic ERGs were measured with 3-ms flashes at an intensity of 30 cd s/m2. Subsequently, photopic ERGs were recorded after a 10-min light adaptation at a flash intensity of 30 cd s/m2 under 30 cd/m2 background light, filtered between 0.3 and 500 Hz. Thirty-two measurements were obtained during the photopic ERG recording and averaged.

For statistical analysis, the amplitudes of a-waves were measured from the baseline to the peak in the cornea-negative direction; those of b-waves were measured from the cornea-negative peak to the major cornea-positive peak. Photopic peak responses were measured from the baseline to the maximum cornea-positive peak. This entire analysis was performed using SCOPE 3 Version 3.8.2 software (AD Instruments).

2.5 Optical coherence tomography (OCT)

Sectional images of the central 30° of the retina were acquired using spectral domain optical coherence tomography (SD-OCT; Heidelberg Engineering,

Heidelberg, Germany). Twelve radial scans centered on the optic nerve were obtained. The whole retinal thickness was measured from the internal limiting membrane to Bruch's membrane at a total of 24 points 2000 μm from the optic nerve, and the values were averaged for analysis.

2.6 Histologic analysis

The eyes were enucleated, fixed with 4% paraformaldehyde, and embedded in paraffin. Vertical sections of 4-μm thickness were made through the optic disks. Specimens were stained with hematoxylin and eosin and photographed under a microscope with a ×20 objective lens (Axio Imager; Carl Zeiss Meditec, Jena, Germany). The thickness of the outer nuclear layer (ONL) of the superior and inferior retina was measured at 250, 750, 1250, and 1750 μm from the optic disk. The number of nuclei in the ONL of the superior and inferior retina at 500 μm–740 μm from the optic disk was counted and averaged for analysis.

2.7 TUNEL assay and quantitative analysis

Photoreceptor apoptosis was determined by terminal deoxynucleotide transferase nick end labelling (TUNEL) using an ApopTag® Peroxidase In Situ Apoptosis Detection Kit (MILLIPORE, Billerica, MA, USA). Diaminobenzidine was used as colour substrate. The number of TUNEL-positive nuclei and the total number of photoreceptor nuclei within 1 section of the ONL of the superior and inferior retina 500 μm to 740 μm from the optic disc were counted and averaged for analysis. The ratio of TUNEL-positive photoreceptor nuclei to total photoreceptor cells was determined.

2.8 Immunohistochemistry on retinal whole-mounts

Retinas were fixed with 4% paraformaldehyde and methanol and blocked in 50% fetal bovine serum/20% normal goat serum for 1 h at room temperature. To stain the microglia, anti-F4/80 (Serotec, Oxford, UK) and Alexa 488-conjugated anti-rat (Invitrogen, Eugene, OR) antibodies were used as the primary and secondary antibodies, respectively. Images were obtained using a confocal microscope (LSM 5Pascal; Carl Zeiss Japan, Tokyo, Japan) with a ×20 objective lens. The number of F4/80-positive cells within four 560 × 560 μm (512 × 512 pixel) squares located at 500 μm from the center of the optic disk was counted and averaged over 4 independent fields.

2.9 Statistical analysis

Statistical analysis was performed using commercial software (SPSS, Chicago, IL). Data from each group were compared using one-way ANOVA followed by the Dunnett test or unpaired t-test, as appropriate.

3. Results

3.1 Chemokine expression in rd10 retinas

In the rd10 mice, photoreceptor cell death began around P18 and peaked on P25 (Fig. 1A, left panel). Most of the photoreceptors were lost by 5 weeks of age (Fig. 1B and C, left panels). Rearing the mice in the dark prevented degeneration as reported previously (Chang et al., 2007) and resulted in thicker photoreceptor layers at each time point (Fig. 1A–C, right panels).

In the control C57BL/6 mice, the expression level of MCP-1 mRNA was low

and did not change with age (Fig. 1D, blue squares, in web version). In contrast, the expression level of MCP-1 mRNA in the retinas of the rd10 mice increased with age, peaking on P24 (Fig. 1D, green squares, in web version). The MCP-1 expression level in rd10 mice was more than 30 times that in the control mice on P24 and remained high through at least P36 (Fig. 1D). The expression pattern of MCP-1 in the dark-reared rd10 mice was different from that of their counterparts reared in a 12-h dark/light cycle. The peak expression shifted to a later time point (P30), and the maximal expression was lower in the former than in the latter (Fig. 1D, purple squares, in web version).

The expression pattern of another CC chemokine RANTES was similar to that of MCP-1 (Fig. 1E: normal rd10, green squares; dark-reared rd10, purple squares, in web version).

The expression level of the CXC chemokine SDF-1 in rd10 mice increased gradually with age, beginning on P33, peaking on P36, and then decreasing to a level similar to that in the control mice by P60 (Fig. 1F, green squares, in web version). The peak SDF-1 expression shifted to a later time point (P45) in the dark-reared rd10 mice, and SDF-1 expression in these mice remained significantly higher than that in the control mice until at least P60 ($P = 0.01$, Fig. 1F, purple squares, in web version).

3.2 Role of the MCP-1/CCR2 system in retinal degeneration in rd10 mice

To assess the role of MCP-1 in retinal degeneration in vivo, we crossed MCP-1 receptor ccr2−/− mice with rd10 mice to generate ccr2−/− rd10 mice (See

Supplementary Fig. S1). According to the genotyping results, we selected ccr2−/− rd10 and ccr2+/+ rd10 mice for our studies. In the ccr2−/− mice, some population of macrophages and other CCR2-positive monocyte-derived cells might fail to migrate in response to MCP-1. Thus, in the ccr2−/− rd10 mice, MCP-1 might not work as a chemotactic cytokine for such cells in the retina.

The whole retinal thickness was measured in live mice at 24 points at 2000 μm from the optic nerve head for each eye (Fig. 2A, in web version). The average retinal thickness did not change over time in the background strain C57BL/6 (Fig. 2B, blue line, in web version), but it gradually decreased in rd10 (Fig. 2B, green line, in web version). Although ccr2−/− rd10 (Fig. 2B, red line, in web version) mice also showed retinal thinning, the thickness was consistently and significantly greater than that in the rd10 mice (P = 0.03 on P24 and P = 0.02 on P30).

3.3 Histological analysis

Histological analysis confirmed that ONL thickness did not change over time in the C57BL/6 mice but decreased in *rd10* and CCR2$^{-/-}$ *rd10* mice (Figure 2D, 2E, and 2F). The ONL was also consistently and significantly thicker in c*cr2*$^{-/-}$ *rd10* mice than in *rd10* mice (*P* = 0.03 at P24 and *P* = 0.03 at P30) (Figure 2G). The average number of ONL cells showed similar pattern and differed between the *rd10* and *ccr2*$^{-/-}$ *rd10* mice at P24 (*P* = 0.03) and P30 (*P* = 0.04)(Figure 2H).

3.4 Investigation of retinal function using ERG.

Under dark-adapted (Fig. 3A–C) and light-adapted (Fig. 3D–F) conditions,

the ERG amplitude was lower in the rd10 and ccr2−/− rd10 mice than in the C57BL/6 mice at all time points. Although the ccr2−/− rd10 mice also showed a time-dependent decrease in the a-wave and b-wave amplitudes (Fig. 3G and H, red line, in web version), these amplitudes were significantly higher than those in the rd10 mice (Fig. 3G and H, green line, in web version) (P24: a-wave, $P = 0.04$ and b-wave, $P = 0.04$; P30: a-wave, $P = 0.01$ and b-wave, $P = 0.02$). The peak wave amplitude of the light-adapted ERG is shown in Fig. 3I. The amplitude was again higher in the ccr2−/− rd10 mice than in the rd10 mice on P24 and P30 ($P = 0.04$ and $P = 0.04$, respectively). These results suggested that ccr2 knockout in rd10 mice resulted in alleviation of photoreceptor cell death both morphologically and functionally.

3.5 Number of macrophages or microglia in the retinas of ccr2-/- rd10 mice

Many F4/80-positive cells were observed in P25 rd10 retinas (Fig. 4A). The number of retinal F4/80-positive cells was significantly smaller in ccr2−/− rd10 mice than in rd10 mice (Fig. 4B and C). These results indicate that the MCP-1/CCR2 system is involved in mobilizing this cell population into the degenerating retinas of rd10 mice.

3.6 Photoreceptor cell apoptosis in rd10 mice was reduced by ccr2 knockout

We counted apoptotic cells in the retinas using the TUNEL assay. As shown in Fig. 4D and E, the number of apoptotic cells on P25 was significantly lower in the ccr2−/− rd10 mice than in the rd10 mice ($P < 0.01$, Fig. 4F). Retinal degeneration progressed and the number of total ONL cells decreased, and on

P30, there were more apoptotic cells in the ONLs of ccr2−/− rd10 mice than rd10 mice ($P < 0.01$, Fig. 4F).

3.7 ccr2 knockout diminishes the increased MCP-1 mRNA expression but does not alter RANTES or TNF-α expression in rd10 retinas

As stated above, MCP-1 mRNA expression was increased in the rd10 retinas (Fig. 1D). However, this increase was not observed in the retinas of ccr2−/− rd10 mice; the MCP-1 mRNA expression levels in these mice were non-significantly different compared to those in the control strain (Fig. 4G).

In contrast to MCP-1 expression, the RANTES or TNF-α mRNA expression levels were similar between ccr2−/− rd10 and rd10 mice, and the differences were not significant (Fig. 4H and I).

4. Discussion

We bred ccr2−/− rd10 mice in order to investigate the roles of the MCP-1/CCR2 system in retinal degeneration. CCR2 knockout alleviated the retinal degeneration, and this result was confirmed via morphologic and functional studies. Although the exact mechanism underlying this protective effect is not clear, the smaller number of microglia-like cells in the ccr2−/− rd10 mice suggested that these cells were in some way involved.

Although increased expression of chemokines has been reported in retinal degeneration (Zeng et al., 2005), it remains unclear whether this change is induced along with retinal degeneration or with other factors including developmental changes. To better understand the association between retinal

degeneration and chemokine expression, we used a dark-reared rd10 model, which facilitates slower retinal degeneration in the same mouse strain (Chang et al., 2007). The expression peak of each chemokine was delayed in the dark-reared mice. The results supported the hypothesis that the increase in the expression of the abovementioned chemokines is induced along with genetic retinal degeneration. The degeneration of photoreceptor was quick and most of the photoreceptor cells were not observed in normally reared rd10. In contrast the degeneration of the dark reared rd10 was very slow and many of the photoreceptors could be observed at P36, when only single layer of photoreceptor was survived in normally reared mice (Fig. 1C). Although the expression peak of MCP-1 was shifted to the later time point in the dark reared rd10 mice, the reduction of MCP-1 expression after the peak was similarly fast as the normally reared mice (Fig. 1D). The results suggest that the induction of MCP-1 is along with the retinal degeneration but not along with the number of survived photoreceptor cells. As discussed later, the presence of positive feedback loop between chemokine upregulation and the incorporated BM-derived cells is one possible mechanism of the chemokine expression profile in the degenerating retina. Although it is difficult to imagine that light can directly influence the expression of chemokines in the retina, it is true that light exposure can influence the neural inflammation of retinal degeneration.

To evaluate the role of the MCP1/CCR2 system in retinal degeneration, we compared ccr2−/− rd10 and normal rd10 mice (ccr2+/+ rd10). Morphological

and functional analysis showed that ccr2 knockout resulted in slower retinal degeneration. Conversely, the upregulation of MCP1/CCR2 in response to retinal degeneration may result in further detrimental effects. The involvement of chronic inflammation in the pathogenesis of chronic neural degeneration, including hereditary retinal degeneration, has been suggested and investigated (Sriram, 2011). Although chemokines and the recruited microglia/macrophages are considered to be key factors in the degeneration process, the details of the mechanism remain unclear. The homeostatic chemokine SDF-1 and its receptor CXCR4 are reported to be involved in tissue repair via their direct chemotactic recruitment of hematopoietic progenitor cells, CD11b+ monocytes/macrophages, and/or tissue-specific stem cells to the sites of injury (Kioi et al., 2010; Kollet et al., 2003; Ratajczak et al., 2003). We previously showed the rescue effect of BM-derived cells and the neuroprotective role of the SDF-1/CXCR4 system in photoreceptor degeneration in rd10 mice (Otani et al., 2002; Otani et al., 2004; Sasahara et al., 2008). Our results suggest that the MCP-1/CCR2 system plays a different role from that played by SDF-1 in retinal degeneration. Because resident microglial cells do not express CCR2 (Mizutani et al., 2012) and the recruitment of circulating myeloid cells into the retina is reported to be via the CCL2-CCR2 pathway (Chen et al., 2012), one possible mechanism that could explain our results is deterioration of microglial recruitment by ccr2 knockout. In fact, we found that the number of F4/80-positive cells was lower smaller in

ccr2−/− rd10 mice than in rd10 mice. It is also possible that the expression of factors that affect photoreceptor survival is altered by ccr2 knockout. Macrophages/microglia secrete several cytokines, including cytotoxic cytokines (Raivich et al., 1999) such as TNF-α, that have been suggested to be important in degenerative diseases of the CNS (Gregersen et al., 2000; Nguyen and Benveniste, 2002). Chen et al. (2012) reported that monocytes from CCR2-deficient mice exhibit enhanced TNF-α expression, which may result in dysregulation of age-related retinal para-inflammatory responses. TNF-α expression was not different in the ccr2−/− rd10 mouse retinas than that in the rd10 mice retinas (Fig. 4I), suggesting that TNF-α may not play an important role in the phenomenon observed in the ccr2−/− rd10 mouse retinas. It is interesting to note that the role of CCR2 seems to be the opposite in age-related retinal changes (Chen et al., 2012) and inherited retinal degeneration. Further studies including investigations with other retinal degeneration models are required to understand the exact role played by CCR2 in retinal degeneration.

Another interesting result is that the induction of MCP-1 mRNA expression but not RANTES or SDF in rd10 mouse retinas was diminished by ccr2 knockout. The result suggests that MCP-1 expression in the degenerating retina may be independently controlled and requires CCR2-positive cells that might be from the BM. There may be a positive feedback loop between MCP-1 upregulation and the incorporation of BM-derived CCR2-positive cells in the degenerating

retina. Further, in ccr2−/− rd10 mice, the initial increase in MCP-1 expression was not even observed in the degenerating retina. The result raises a question about the role of tissue-resident cells including microglia. CNS tissue-resident microglia/macrophages (Schilling et al., 2003) are thought to be involved in the initial steps of infection, injury, or inflammation in neural tissues. Activation of tissue-resident microglia has been suggested to precede recruitment of BM-derived monocytes and their subsequent differentiation into microglia (Streit, 2002; Tanaka et al., 2003; Vallieres and Sawchenko, 2003); interestingly, our results did not support this hypothesis.

Chemokines play important roles in the recruitment of BM-derived cells into the tissue under pathological conditions. In the inherited degenerating retina examined using rd10 mice, MCP-1 and SDF-1 showed different expression profiles with different roles during degeneration. Further studies are required to clarify the roles of chemokines and microglia in neural degeneration, and we hope that this investigation will assist in the development of effective therapies for currently intractable diseases.

References

Bennett, L.D., Fox, J.M., Signoret, N., 2011. Mechanisms regulating chemokine receptor activity. Immunology 134, 246-256.
Chang, B., Hawes, N.L., Pardue, M.T., German, A.M., Hurd, R.E., Davisson, M.T., Nusinowitz, S., Rengarajan, K., Boyd, A.P., Sidney, S.S., Phillips, M.J., Stewart, R.E., Chaudhury, R., Nickerson, J.M., Heckenlively, J.R., Boatright, J.H., 2007. Two mouse retinal degenerations caused by missense mutations in the beta-subunit of rod cGMP phosphodiesterase gene. Vision Res 47, 624-633.
Chen, H., Liu, B., Lukas, T.J., Neufeld, A.H., 2008. The aged retinal pigment epithe- lium/choroid: a potential substratum for the pathogenesis of age-related macular degeneration. PLoS One 3, e2339.
Chen, M., Zhao, J., Luo, C., Pandi, S.P., Penalva, R.G., Fitzgerald, D.C., Xu, H., 2012. Para-inflammation-mediated retinal recruitment of bone marrow-derived myeloid cells following whole-body irradiation is CCL2 dependent. Glia 60, 833-842.
Conductier, G., Blondeau, N., Guyon, A., Nahon, J.L., Rovere, C., 2010. The role of monocyte chemoattractant protein MCP1/CCL2 in neuroinflammatory diseases. J. Neuroimmunol. 224, 93-100.
Coughlan, C.M., McManus, C.M., Sharron, M., Gao, Z., Murphy, D., Jaffer, S., Choe, W., Chen, W., Hesselgesser, J., Gaylord, H., Kalyuzhny, A., Lee, V.M., Epstein, L.G., 1998. HIV neuropathogenesis and therapeutic strategies. Acta Paediatr Jpn 40, 107-111.
Fife, B.T., Huffnagle, G.B., Kuziel, W.A., Karpus, W.J., 2000. CC chemokine receptor 2 is critical for induction of experimental autoimmune encephalomyelitis. J Exp Med 192, 899-905.
Frossard, J.L., Lenglet, S., Montecucco, F., Steffens, S., Galan, K., Pelli, G., Spahr, L., Mach, F., Hadengue, A., 2011. Role of CCL-2, CCR-2 and CCR-4 in cerulein-induced acute pancreatitis and pancreatitis-associated lung injury. J Clin Pathol 64, 387-393.
Gerard, C., Rollins, B.J., 2001. Chemokines and disease. Nat Immunol 2, 108-115.
Glabinski, A.R., Balasingam, V., Tani, M., Kunkel, S.L., Strieter, R.M., Yong, V.W., Ransohoff, R.M., 1996. Chemokine monocyte chemoattractant protein-1 is expressed by astrocytes after mechanical injury to the brain. J Immunol 156, 4363-4368.
Gourmala, N.G., Buttini, M., Limonta, S., Sauter, A., Boddeke, H.W., 1997. Differential and time-dependent expression of monocyte chemoattractant protein-1 mRNA by astrocytes and macrophages in rat brain: effects of ischemia and peripheral lipopolysaccharide administration. J Neuroimmunol 74, 35-44.
Gregersen, R., Lambertsen, K., Finsen, B., 2000. Microglia and macrophages

are the major source of tumor necrosis factor in permanent middle cerebral artery occlusion in mice. J Cereb Blood Flow Metab 20, 53-65.
Gu, L., Tseng, S.C., Rollins, B.J., 1999. Monocyte chemoattractant protein-1. Chem Immunol 72, 7-29.
Harada, T., Harada, C., Kohsaka, S., Wada, E., Yoshida, K., Ohno, S., Mamada, H., Tanaka, K., Parada, L.F., Wada, K., 2002. Microglia-Muller glia cell interactions control neurotrophic factor production during light-induced retinal degeneration. J Neurosci 22, 9228-9236.
Hartong, D.T., Berson, E.L., Dryja, T.P., 2006. Retinitis pigmentosa. Lancet 368, 1795-1809.
Hickman, S.E., El Khoury, J., 2010. Mechanisms of mononuclear phagocyte recruitment in Alzheimer's disease. CNS Neurol Disord Drug Targets 9, 168-173.
Huang, D., Han, Y., Rani, M.R., Glabinski, A., Trebst, C., Sorensen, T., Tani, M., Wang, J., Chien, P., O'Bryan, S., Bielecki, B., Zhou, Z.L., Majumder, S., Ransohoff, R.M., 2000. Chemokines and chemokine receptors in inflammation of the nervous system: manifold roles and exquisite regulation. Immunol Rev 177, 52-67.
Huang, D.R., Wang, J., Kivisakk, P., Rollins, B.J., Ransohoff, R.M., 2001. Absence of monocyte chemoattractant protein 1 in mice leads to decreased local macrophage recruitment and antigen-specific T helper cell type 1 immune response in experimental autoimmune encephalomyelitis. J Exp Med 193, 713-726.
Izikson, L., Klein, R.S., Charo, I.F., Weiner, H.L., Luster, A.D., 2000. Resistance to experimental autoimmune encephalomyelitis in mice lacking the CC chemokine receptor (CCR)2. J Exp Med 192, 1075-1080.
Kim, M.S., Day, C.J., Morrison, N.A., 2005. MCP-1 is induced by receptor activator of nuclear factor-{kappa}B ligand, promotes human osteoclast fusion, and rescues granulocyte macrophage colony-stimulating factor suppression of osteoclast formation. J Biol Chem 280, 16163-16169.
Kioi, M., Vogel, H., Schultz, G., Hoffman, R.M., Harsh, G.R., Brown, J.M., 2010. Inhibition of vasculogenesis, but not angiogenesis, prevents the recurrence of glioblastoma after irradiation in mice. J Clin Invest 120, 694-705.
Kollet, O., Shivtiel, S., Chen, Y.Q., Suriawinata, J., Thung, S.N., Dabeva, M.D., Kahn, J., Spiegel, A., Dar, A., Samira, S., Goichberg, P., Kalinkovich, A., Arenzana-Seisdedos, F., Nagler, A., Hardan, I., Revel, M., Shafritz, D.A., Lapidot, T., 2003. HGF, SDF-1, and MMP-9 are involved in stress-induced human CD34+ stem cell recruitment to the liver. J Clin Invest 112, 160-169.
Lawrence, D.A., Kim, D., 2000. Central/peripheral nervous system and immune responses. Toxicology 142, 189-201.
Luster, A.D., 1998. Chemokines--chemotactic cytokines that mediate inflammation. N Engl J Med 338, 436-445.
Ma, W., Zhao, L., Fontainhas, A.M., Fariss, R.N., Wong, W.T., 2009. Microglia in the mouse retina alter the structure and function of retinal pigmented

epithelial cells: a potential cellular interaction relevant to AMD. PLoS One 4 (11), e7945.
Matyszak, M.K., 1998. Inflammation in the CNS: balance between immunological privilege and immune responses. Prog Neurobiol 56, 19-35.
Mizutani, M., Pino, P.A., Saederup, N., Charo, I.F., Ransohoff, R.M., Cardona, A.E., 2012. The fractalkine receptor but not CCR2 is present on microglia from embryonic development throughout adulthood. J. Immunol. 188, 29-36.
Moser, B., Wolf, M., Walz, A., Loetscher, P., 2004. Chemokines: multiple levels of leukocyte migration control. Trends Immunol 25, 75-84.
Nakazawa, T., Hisatomi, T., Nakazawa, C., Noda, K., Maruyama, K., She, H., Matsubara, A., Miyahara, S., Nakao, S., Yin, Y., Benowitz, L., Hafezi-Moghadam, A., Miller, J.W., 2007. Monocyte chemoattractant protein 1 mediates retinal detachment-induced photoreceptor apoptosis. Proc. Natl. Acad. Sci. U. S. A. 104, 2425-2430.
Nguyen, V.T., Benveniste, E.N., 2002. Critical role of tumor necrosis factor-alpha and NF-kappa B in interferon-gamma -induced CD40 expression in microglia/macrophages. J Biol Chem 277, 13796-13803.
Otani, A., Dorrell, M.I., Kinder, K., Moreno, S.K., Nusinowitz, S., Banin, E., Heckenlively, J., Friedlander, M., 2004. Rescue of retinal degeneration by intravitreally injected adult bone marrow-derived lineage-negative hematopoietic stem cells. J Clin Invest 114, 765-774.
Otani, A., Kinder, K., Ewalt, K., Otero, F.J., Schimmel, P., Friedlander, M., 2002. Bone marrow-derived stem cells target retinal astrocytes and can promote or inhibit retinal angiogenesis. Nat Med 8, 1004-1010.
Raine, C.S., 1994. Multiple sclerosis: immune system molecule expression in the central nervous system. J Neuropathol Exp Neurol 53, 328-337.
Raivich, G., Bohatschek, M., Kloss, C.U., Werner, A., Jones, L.L., Kreutzberg, G.W., 1999. Neuroglial activation repertoire in the injured brain: graded response, molecular mechanisms and cues to physiological function. Brain Res Brain Res Rev 30, 77-105.
Ratajczak, M.Z., Majka, M., Kucia, M., Drukala, J., Pietrzkowski, Z., Peiper, S., Janowska-Wieczorek, A., 2003. Expression of functional CXCR4 by muscle satellite cells and secretion of SDF-1 by muscle-derived fibroblasts is associated with the presence of both muscle progenitors in bone marrow and hematopoietic stem/progenitor cells in muscles. Stem Cells 21, 363-371.
Saijo, K., Glass, C.K., 2011. Microglial cell origin and phenotypes in health and disease. Nat. Rev. Immunol. 11, 775-787.
Sasahara, M., Otani, A., Oishi, A., Kojima, H., Yodoi, Y., Kameda, T., Nakamura, H., Yoshimura, N., 2008. Activation of bone marrow-derived microglia promotes photoreceptor survival in inherited retinal degeneration. Am J Pathol 172, 1693-1703.
Schilling, M., Besselmann, M., Leonhard, C., Mueller, M., Ringelstein, E.B., Kiefer, R., 2003. Microglial activation precedes and predominates over

macrophage infiltration in transient focal cerebral ischemia: a study in green fluorescent protein transgenic bone marrow chimeric mice. Exp Neurol 183, 25-33.
Semple, B.D., Bye, N., Rancan, M., Ziebell, J.M., Morganti-Kossmann, M.C., 2010. Role of CCL2 (MCP-1) in traumatic brain injury (TBI): evidence from severe TBI patients and CCL2-/- mice. J Cereb Blood Flow Metab 30, 769-782.
Simpson, J.E., Newcombe, J., Cuzner, M.L., Woodroofe, M.N., 1998. Expression of monocyte chemoattractant protein-1 and other beta-chemokines by resident glia and inflammatory cells in multiple sclerosis lesions. J Neuroimmunol 84, 238-249.
Simpson, J.E., Newcombe, J., Cuzner, M.L., Woodroofe, M.N., 1998. Expression of monocyte chemoattractant protein-1 and other beta-chemokines by resident glia and inflammatory cells in multiple sclerosis lesions. J. Neuroimmunol. 84, 238-249.
Sriram, S., 2011. Role of glial cells in innate immunity and their role in CNS demyelination. J. Neuroimmunol. 239, 13-20.
Streit, W.J., 2002. Microglia and the response to brain injury. Ernst Schering Res Found Workshop, 11-24.
Tanaka, R., Komine-Kobayashi, M., Mochizuki, H., Yamada, M., Furuya, T., Migita, M., Shimada, T., Mizuno, Y., Urabe, T., 2003. Migration of enhanced green fluorescent protein expressing bone marrow-derived microglia/macrophage into the mouse brain following permanent focal ischemia. Neuroscience 117, 531-539.
Vallieres, L., Sawchenko, P.E., 2003. Bone marrow-derived cells that populate the adult mouse brain preserve their hematopoietic identity. J Neurosci 23, 5197-5207.
Xia, M.Q., Hyman, B.T., 1999. Chemokines/chemokine receptors in the central nervous system and Alzheimer's disease. J Neurovirol 5, 32-41.
Zeng, H.Y., Zhu, X.A., Zhang, C., Yang, L.P., Wu, L.M., Tso, M.O., 2005. Identification of sequential events and factors associated with microglial activation, migration, and cytotoxicity in retinal degeneration in rd mice. Invest Ophthalmol Vis Sci 46, 2992-2999.
Zola, H., Swart, B., Boumsell, L., Mason, D.Y., Subcommittee I.W., 2003. Human Leukocyte Differentiation Antigen Nomenclature: update on CD nomenclature. Report of IUIS/WHO subcommittee. J. Immunol. Methods 275, 1-8.

Figure Legends

Figure 1. Histological sections of rd10 mice on P24 (A), P30 (B), and P36 (C). The photographs in each panel on the left represent animals reared under a 12-h light/dark cycle, and the ones on the right represent those reared under 24-h darkness. GCL, ganglion cell layer; INL, inner nuclear layer; ONL, outer nuclear layer. Changes in the relative expression levels of MCP-1 (D). The degenerating retina of rd10 mice showed increased MCP-1 expression, with a peak on P24. Note that in the dark-reared mice, the peak was on P30 and the maximal expression level was lower. The RANTES expression levels showed a similar pattern (E). SDF-1 expression was also increased in the degenerating retinas of the rd10 mice, but the peak expression was noted on P36, 12 days later than when it was observed for MCP-1 and RANTES, and the peak shifted to P45 for the dark-reared rd10 mice (F). Scale bars = 20 μm (A–C). n = 6 mice at each time point per group. Error bars represent SD (D–E).

Figure 2. Representative figures for OCT measurement. Twelve lines of radial scans centering on the optic nerve were made. The total retinal thickness was measured at 2000 μm from the optic nerve in each scan, and the data from 12 scans were averaged and compared among wild-type, ccr2−/− rd10, and ccr2+/+ rd10 mice (A). ILM, internal limiting membrane; BM, Bruch's membrane. Although both groups of rd10 mice showed decreased retinal thickness, the decrease was more severe in the ccr2+/+ rd10 mice on P24 and P30 (B). This result was also confirmed by histological analysis (C, D, and E).

GCL, ganglion cell layer; INL, inner nuclear layer; ONL, outer nuclear layer. Both the outer nuclear thickness (F and G) and the number of nuclei in the outer nuclear layer (H) and the expression of rhodopsin (I) were lower in the ccr2+/+ rd10 mice on P24 and P30. *P < 0.05, **P < 0.01. Scale bars = 20 μm (C–E). n = 8 mice at each time point per group. Error bars represent SD (B, F, G, H and I).

Figure 3. Representative electroretinogram (ERG) data (A–F). compared with WT mice, rd10 mice showed decreased amplitude in all settings under all conditions except for the photopic ERG recorded on P18 (G–I). The amplitudes on P24 and P30 were relatively preserved in the ccr2−/− mice compared with the ccr2+/+ mice. *P < 0.05, **P < 0.01. n = 8 mice at each time point per group. Error bars represent SD (G–I).

Figure 4. Microglia migrating into the ccr2+/+ rd10 (A) and ccr2−/− rd10 (B) retinas were stained with F4/80 and counted on retinal flat mounts. The number of microglia in the superficial layer of vasculature was significantly lower in the ccr2−/− retinas (C). Apoptotic cells were also counted using TUNEL staining (D, E). GCL, ganglion cell layer; INL, inner nuclear layer; ONL, outer nuclear layer. The percentage of TUNEL-positive cells was lower in the ccr2−/− rd10 mice than in the ccr2+/+ rd10 mice on P25 but it increased on P30, probably due to the later peak of degeneration (F). The MCP-1 expression level was not increased in the ccr2−/− rd10 mice and was similar to that of the control B6 mice at all time points (G). RANTES expression levels

were also not different in the ccr2−/− rd10 mice from those in the ccr2+/+ rd10 mice at any time point (H). The degenerating retinas of the ccr2+/+ rd10 mice showed increased expression of TNF-α, peaking on P24, similar to the ccr2−/− rd10 mice. *P < 0.05, **P < 0.01. Scale bars = 50 μm (A and B) or 20 μm (D and E). n = 6 mice at each time point per group (C, F); n = 8 mice at each time point per group (G–I). Error bars represent SD (C, F, and G–H).

Supplementary material

Figure S1. ccr2 genotypes (A). Lane 2 shows the 424-bp band produced from ccr2+/+ rd10 mice and lane 3 the 280-bp band produced from ccr2-/- B6 mice. Both of these bands were observed for crossbred ccr2+/- Pde6b +/- mice. A similar assay was used for Pde6b (B). Line 2 (ccr2-/- B6) shows the 2 fragment bands at 150 and 54 bp and line 3 (rd10) shows the uncleaved 204-bp band. Heterozygosity at Pde6b was confirmed for crossbred mice as shown in line 4. bp: base pair.

Figure 1.

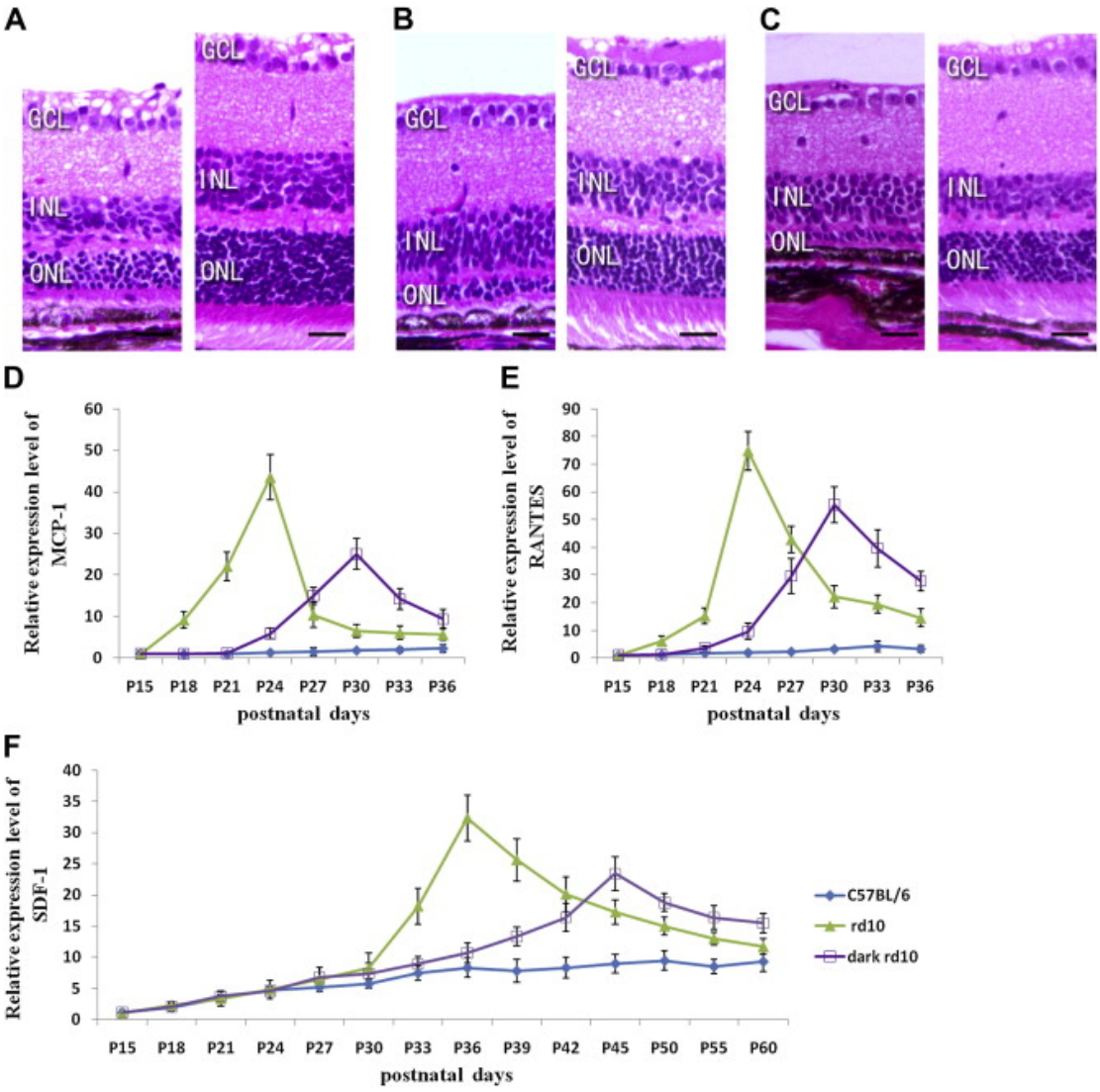
A
B
C
GCL
INL
ONL
D
Relative expression level of MCP-1
E
Relative expression level of RANTES
P15 P18 P21 P24 P27 P30 P33 P36
postnatal days
F
Relative expression level of SDF-1
P15 P18 P21 P24 P27 P30 P33 P36 P39 P42 P45 P50 P55 P60
postnatal days
C57BL/6
rd10
dark rd10

Figure 2.

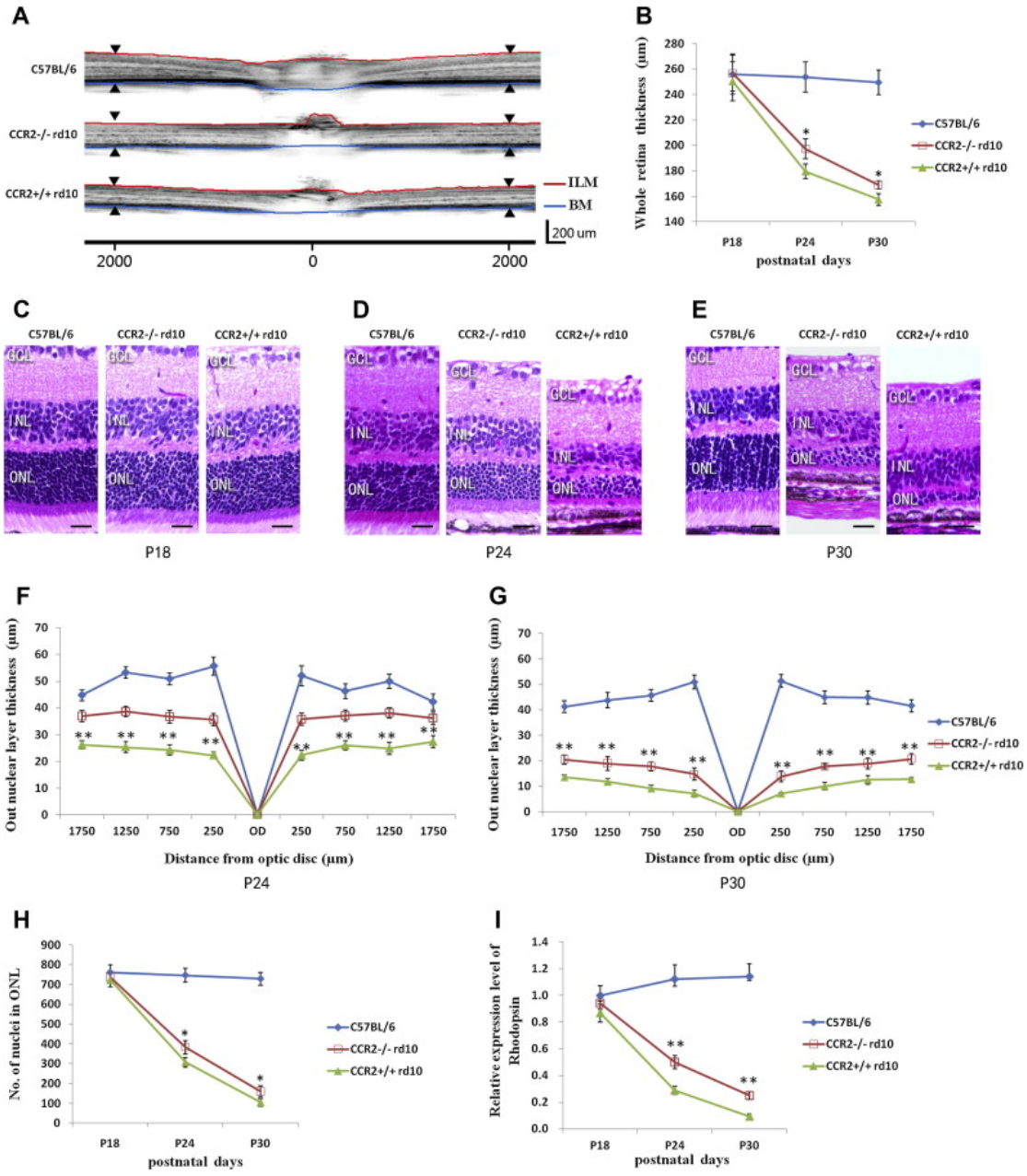
A
C57BL/6
CCR2-/- rd10
CCR2+/+ rd10
ILM
BM
200 um
2000
0
2000
B
Whole retina thickness (μm)
postnatal days
P18
P24
P30
C57BL/6
CCR2-/- rd10
CCR2+/+ rd10
C
D
E
GCL
INL
ONL
P18
P24
P30
F
G
Out nuclear layer thickness (μm)
Distance from optic disc (μm)
1750
1250
750
250
OD
H
No. of nuclei in ONL
I
Relative expression level of Rhodopsin

Figure 3.

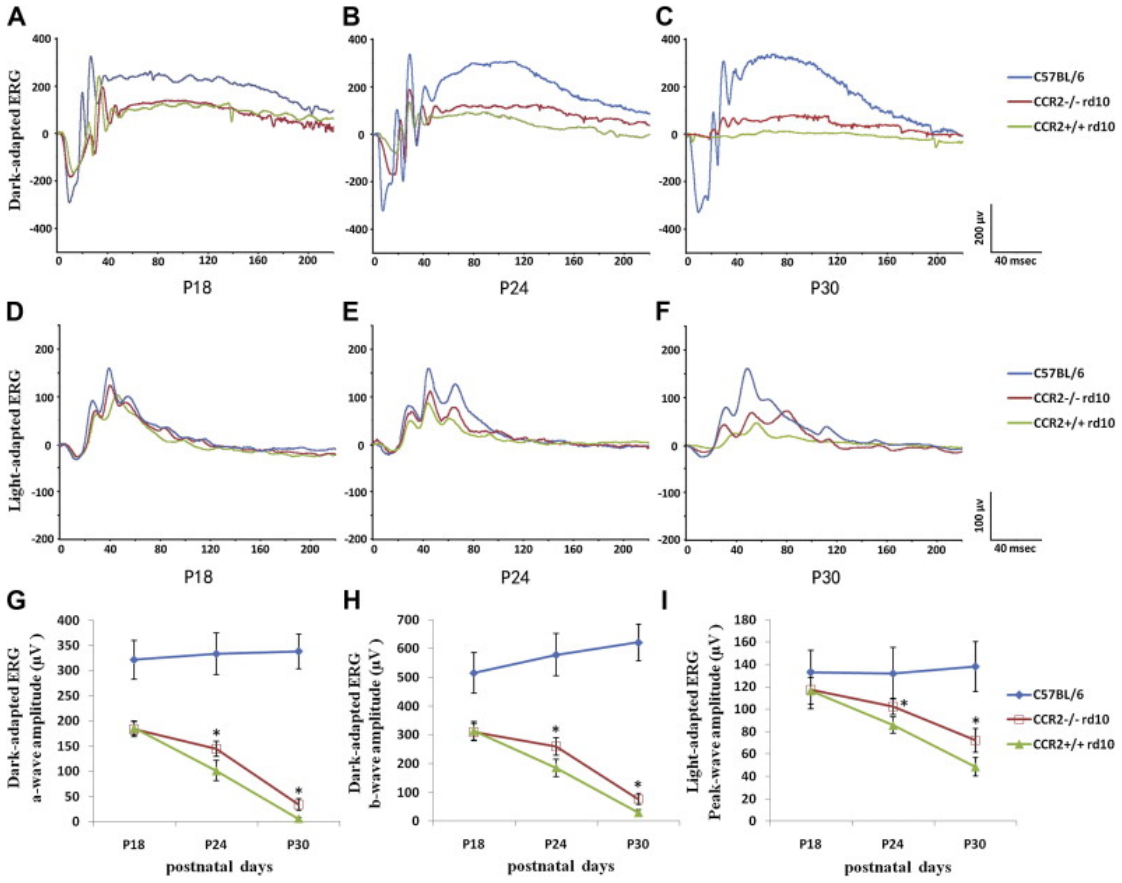
A
B
C
Dark-adapted ERG
P18
P24
P30
C57BL/6
CCR2-/- rd10
CCR2+/+ rd10
200 µv
40 msec
D
E
F
Light-adapted ERG
100 µv
G
H
I
Dark-adapted ERG a-wave amplitude (µV)
Dark-adapted ERG b-wave amplitude (µV)
Light-adapted ERG Peak-wave amplitude (µV)
postnatal days

Figure 4.

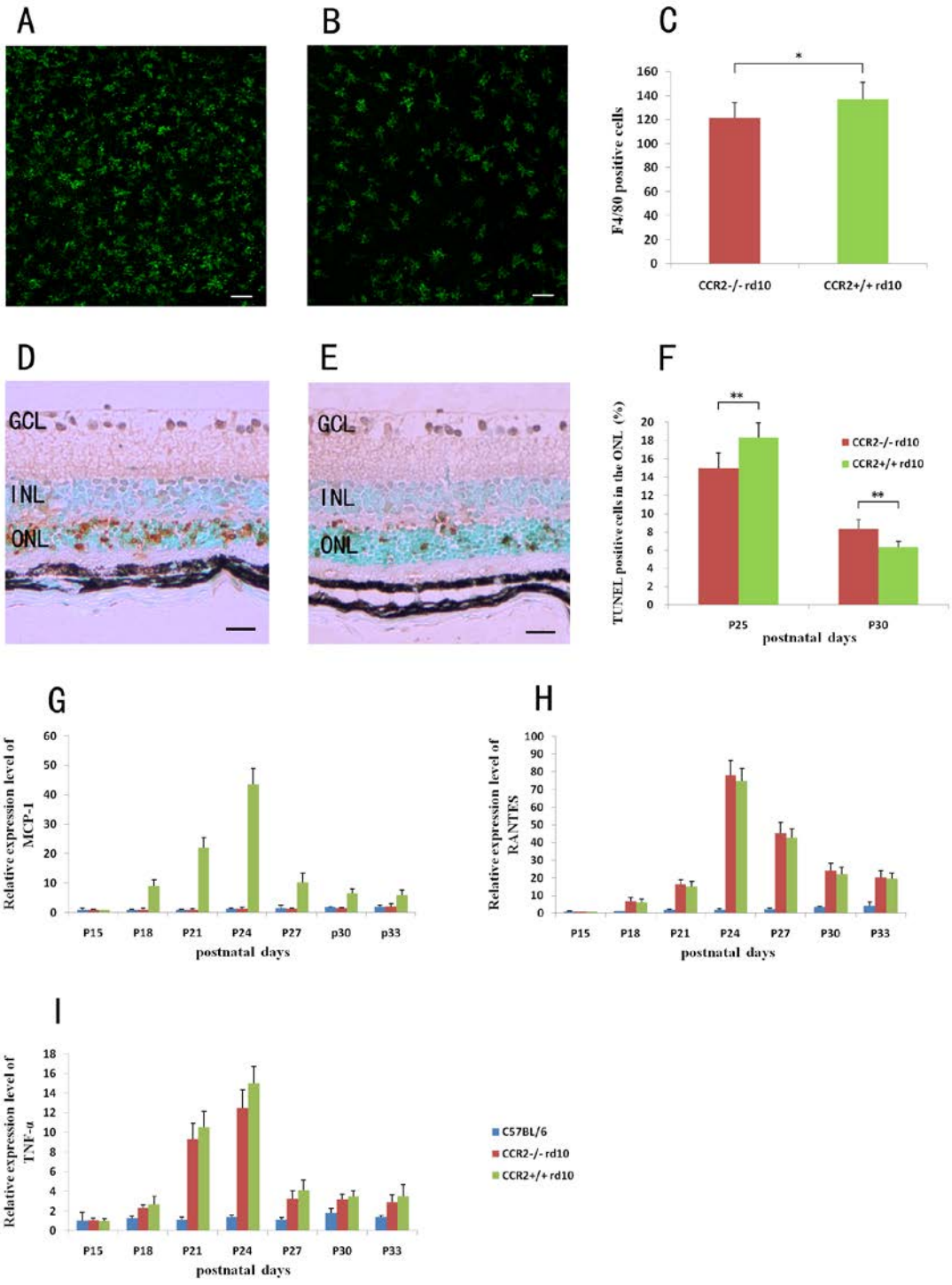
A
B
C
F4/80 positive cells
CCR2-/- rd10
CCR2+/+ rd10
D
E
GCL
INL
ONL
F
TUNEL positive cells in the ONL (%)
postnatal days
P25
P30
G
Relative expression level of MCP-1
H
Relative expression level of RANTES
P15
P18
P21
P24
P27
P30
P33
I
Relative expression level of TNF-α
C57BL/6

Supplementary material

Figure S1.